Spin orders and lattice distortions of geometrically frustrated 6H-perovskites $Ba_3B'Ru_2O_9$ ($B' = La^{3+}$, Nd^{3+}, and Y^{3+})

Mark S. Senn,[1] Simon A. J. Kimber,[2] Angel M. Arevalo Lopez,[1] Adrian H. Hill,[2,*] and J. Paul Attfield[1,†]

[1]*Centre for Science at Extreme Conditions and School of Chemistry, University of Edinburgh, Mayfield Road, Edinburgh EH9 3JZ, United Kingdom*

[2]*ESRF, Boîte Postale 156, F-38042 Grenoble Cedex 9, France*

(Received 25 January 2013; published 2 April 2013)

The magnetic and crystal structures of the title materials have been investigated using high-resolution neutron and synchrotron x-ray powder diffraction. Ferromagnetic Ru dimers are observed in the spin-ordered ground states of all three materials, evidencing an intradimer double exchange interaction. Antiferromagnetic order between dimers breaks the degeneracy of the triangular lattice but no distortion of the $B' =$ La and Y structures is observed. The magnetic ordering transition temperature increases with the radius of the B' cation. An anomalous 120 K structural transition in $Ba_3NdRu_2O_9$ is attributed to Jahn-Teller distortion, evidenced by large-amplitude Γ_6 deformations of the NdO_6 octahedra. Further lattice anomalies accompany magnetic ordering transitions at 24 and 18 K in $Ba_3NdRu_2O_9$. Nd spins order ferromagnetically and a substantial magnetic anisotropy leads to large coercivity and $\frac{1}{3}$-magnetization steps in the magnetic hysteresis loop.

DOI: 10.1103/PhysRevB.87.134402 PACS number(s): 75.25.−j, 75.50.Dd, 75.50.Ee, 64.70.K−

I. INTRODUCTION

The 6H-perovskites, $Ba_3B'Ru_2O_9$, have recently been identified as geometrically frustrated systems,[1] and are potentially suitable materials for observing spin liquid–type behavior,[2] as they contain two-dimensional triangular layers of Ru_2O_9 face-sharing octahedral dimers.[3] Most derivatives adopt the aristotype 6H structure (with hexagonal space group $P6_3/mmc$) as shown in Fig. 1, but those with $B' =$ Sr (Ref. 4) and Cu (Ref. 5) have lower symmetry at ambient conditions. B' cations with odd charge values result in semivalent Ru states so that charge- and spin-ordered ground states may be formed. Charge ordering as $(Ru^{5+})_2O_9$ and $(Ru^{6+})_2O_9$ dimers has recently been reported for $Ba_3NaRu_2O_9$ accompanied by the opening of a spin gap and a structural phase transition at 210 K to monoclinic $P2/c$ symmetry.[6] The opening of a spin gap in $Ba_3BiRu_2O_9$ has also recently been reported,[7] resulting in a phase transition to $C2/c$ symmetry at 176 K.

Magnetic ordering transitions are evident in susceptibility measurements from $Ba_3B'Ru_2O_9$ materials, but spin arrangements have been determined by neutron diffraction only for $B' = Ni^{2+}$ and Co^{2+}.[5,8,9] The $(Ru^{5+})_2O_9$ spin dimers are antiferromagnetic and are coupled to ordered Ni or Co spins. $B' = R^{3+}$ (rare earth) and Y^{3+} materials have Néel transitions at $T_N < 28$ K and remain hexagonal down to 2 K,[3,10] except for $B' = Nd^{3+}$ in which a transition to $C2/c$ symmetry has been reported at 120 K in addition to two low-temperature transitions, at $T_1 = 24$ and $T_2 = 17$ K, observed in magnetization and heat capacity measurements.[11] Broad features in magnetic susceptibility and specific heat measurements at high temperatures were interpreted as evidence for local antiferromagnetic pairing within Ru_2O_9 dimers.[3] Previous neutron powder diffraction data revealed ferromagnetic ordering of Nd^{3+} moment in $Ba_3Nd^{3+}Ru_2O_9$ below T_1, but the nature of the further order at T_2 was unclear.[11] $B' =$ Y and La materials have not been investigated by neutron diffraction. Here we report low-temperature neutron diffraction studies of the spin order in $Ba_3B'Ru_2O_9$ ($B' =$ La, Nd, and Y) which show that the spin dimers are ferromagnetic in all the materials, with no charge order apparent. In the case of $B' = Nd^{3+}$ we find an antiferromagnetic order of the ferromagnetic Ru dimers and canting of Nd moments below T_2. We also evidence local distortions around Nd^{3+} that may drive the 120 K structural transition.

II. EXPERIMENT

Samples of $Ba_3B'Ru_2O_9$ ($B' =$ La, Y, Nd) were prepared by calcining pellets made from stoichiometric amounts of RuO_2, $BaCO_3$, and B'_2O_3 at 900 °C. The pellets were heated to between 1100 °C and 1400 °C for 72 h with multiple cycles of regrinding and repelletization, following previously reported methods of preparation.[3] The samples were found to be phase pure by laboratory x-ray diffraction. High-resolution synchrotron x-ray powder diffraction data [wavelength = 0.399 83(4) Å] were collected from the ID31 beamline at ESRF for $B' =$ La, Y at room temperature and for $B' =$ Nd in the range 10–295 K. High-resolution neutron powder diffraction data were collected for $B' =$ La and Y at the time-of-flight diffractometer HRPD at ISIS from 10 and 2 K, respectively, up to 300 K. Neutron powder diffraction data from all three samples were also measured down to 1.6 K at the time-of-flight neutron powder diffractometer WISH at ISIS up to a d spacing of 30 Å.[12] Magnetization-field hysteresis loops were collected for the $B' =$ Nd samples at 2, 15, 20, 30, and 150 K.

III. RESULTS

A. $Ba_3LaRu_2O_9$ and $Ba_3YRu_2O_9$

Results from refinement of the crystal structures against the ID31 data at 300 K are summarized in Table I, and are consistent with previously published structural models.[3] Additional peaks due to magnetic scattering were observed in the neutron powder diffraction profiles for $B' =$ La and Y samples (Fig. 2) below their respective magnetic transition temperatures of 22 and 4.5 K, previously reported from susceptibility and heat capacity measurements.[10] The

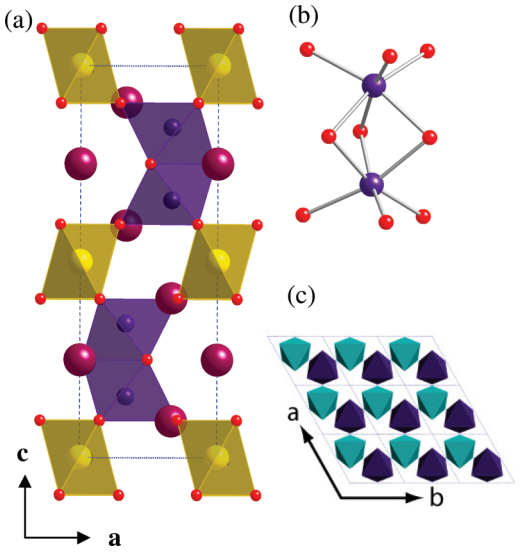

FIG. 1. (Color online) Crystal structure of 6H $Ba_3B'Ru_2O_9$ hexagonal perovskites: (a) projection on the *ac* plane; (b) a Ru_2O_9 dimer; (c) the triangular lattice of Ru_2O_9 dimers with light/dark shading of dimers centered in the $z = \frac{1}{4}/z = \frac{3}{4}$ planes.

magnetic peaks for both materials are indexed by the $(0\ \frac{1}{2}\ 0)$ propagation vector, equivalent to an orthorhombic $a_o = a, b_o = \sqrt{3}a, c_o = c$ *Cmcm* superstructure of the hexagonal $P6_3/mmc$ cell. The irreducible representations and basis vectors of the Ru spins in $P6_3/mmc$ under the propagation vector $(0\ \frac{1}{2}\ 0)$, generated from the program BASIREPS of the FULLPROF suite,[13] are shown in Table II.

Models containing antiferromagnetic Ru_2O_9 spin dimers, as proposed from previous magnetic heat capacity results,[10] did not fit the magnetic intensities of $Ba_3LaRu_2O_9$. However, a model [Fig. 2(b), inset] of ferromagnetic dimers described by the basis vectors from two different representations

TABLE I. Rietveld structural refinement model for $Ba_3B'Ru_2O_9$, $B' =$ La and Y at 11 and 2 K, respectively, against neutron powder diffraction data (from HRPD at ISIS). Refined hexagonal lattice parameters, fractional coordinates, isotropic thermal U factors, and fitting residual wR_p values are shown. Estimated standard deviations are in parentheses. Atomic positions in space group $P6_3/mmc$ are Ba1 (0,0,$\frac{1}{4}$), Ba2 ($\frac{1}{3}$,$\frac{2}{3}$,z), B' (0,0,0), Ru ($\frac{1}{3}$,$\frac{2}{3}$,z), O1 (x,2x, $\frac{1}{4}$), and O2 (x,2x,z).

B'	La	Y
a (Å)	5.9492(1)	5.865 60(9)
c (Å)	14.9981(4)	14.4817(2)
Ba2 z	0.8909(1)	0.9061(1)
Ru z	0.165 56(8)	0.164 18(7)
O1 x	0.4873(1)	0.4892(1)
O2 x	0.178 89(8)	0.176 63(9)
O2 z	0.404 71(4)	0.3532(2)
Ba U_{iso} (Å^2)	0.0081(3)	0.0026(2)
B' U_{iso} (Å^2)	0.0066(3)	0.0026 (3)
Ru U_{iso} (Å^2)	0.0024(2)	0.0016(2)
O U_{iso} (Å^2)	0.0108(2)	0.0060(1)
wR_p (%)	6.66	5.75

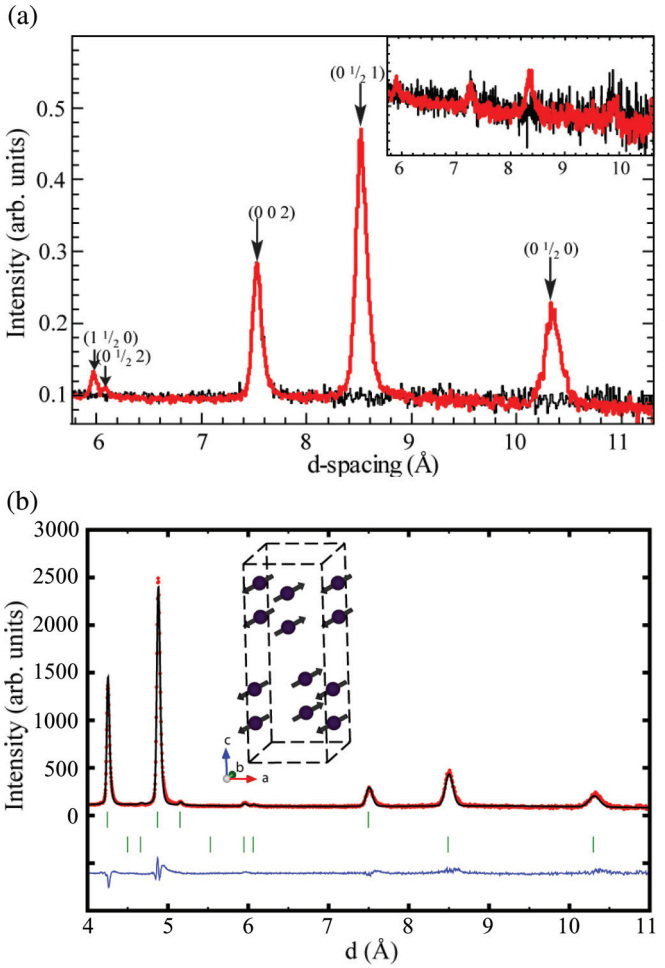

FIG. 2. (Color online) (a) Overlay of neutron diffraction spectra (from WISH at ISIS) for $Ba_3B'Ru_2O_9$ with $B' =$ La at 40 and 10 K (red), with magnetic peaks evident in the latter profile. The inset shows a similar comparison of profiles for the $B' =$ Y analog at 8 and 1.6 K, where less intense magnetic intensities are observed. (b) Rietveld fit to $B' =$ La data at 1.6 K with the magnetic intensities (lower tick marks) modeled by the $(0\ \frac{1}{2}\ 0)$ model shown.

accounts well for the observed magnetic diffraction intensities [Fig. 2(b)]. The $\Psi_1(\Gamma_5)$ basis fits the $(0\ \frac{1}{2}\ l)$ magnetic peaks but predicts zero intensity for the $(1\ \frac{1}{2}\ 0)$ peak which is clearly observed in Fig. 2(a), hence the need for an additional $\Psi_2(\Gamma_3)$ component. $\Psi_1(\Gamma_5)$ and $\Psi_2(\Gamma_3)$ respectively describe Ru spin components parallel to the $\boldsymbol{a_o}$ and $\boldsymbol{c_o}$ vectors of the orthorhombic supercell, with values $m_x = 1.3(1)\mu_B$ and $m_z = 0.6(2)\mu_B$, and resultant moment $1.4(2)\mu_B$, at 1.6 K. The magnetic peaks for $Ba_3YRu_2O_9$ at 1.6 K are less intense and the corresponding refined components are $m_x = 0.4(3)\mu_B$ and $m_z = 0.2(5)\mu_B$, with a resultant moment of $0.5(6)\mu_B$. Although the fitting errors on these values are large, the appearance of the same magnetic reflections including a weak $(1\ \frac{1}{2}\ 0)$ peak [Fig. 2(a), inset] demonstrates that both magnetic bases are present for $Ba_3YRu_2O_9$. The moments in both materials are significantly reduced from the ideal value of $2.5\mu_B$, consistent with a frustrated spin order. Nearest-neighbor Ru-Ru alignments are ferromagnetic along one side and antiferromagnetic on two sides of each plaquette in the

TABLE II. Irreducible representations and basis vectors of the space group $P6_3/mmc$ for the Ru site $(\frac{1}{3},\frac{2}{3},z)$ (where $z = 0.165\,56$ and $0.164\,18$ for $B' =$ La and Y, respectively) under the propagation vector $(0\ \frac{1}{2}\ 0)$. The magnetic structure of $Ba_3LaRu_2O_9$ in Fig. 2(b) is a combination of the basis vectors $\Gamma_3(\Psi_2)$ and $\Gamma_5(\Psi_1)$.

Irreducible representations	Basis vectors	x, y, z			$-x,-y, z+\frac{1}{2}$			$x-y, -y,-z$			$-x+y, y,-z+\frac{1}{2}$		
		m_x	m_y	m_z	m_x	m_y	m_z	m_x	m_y	m_z	m_x	m_y	m_z
Γ_1	Ψ_1	1	0	0	−1	0	0	1	0	0	−1	0	0
Γ_2	Ψ_1	1	2	0	−1	−2	0	−1	−2	0	1	2	0
	Ψ_2	0	0	1	0	0	1	0	0	−1	0	0	−1
Γ_3	Ψ_1	1	2	0	−1	−2	0	1	2	0	−1	−2	0
	Ψ_2	0	0	1	0	0	1	0	0	1	0	0	1
Γ_4	Ψ_1	1	0	0	−1	0	0	−1	0	0	1	0	0
Γ_5	Ψ_1	1	0	0	1	0	0	1	0	0	1	0	0
Γ_6	Ψ_1	1	2	0	1	2	0	−1	−2	0	−1	−2	0
	Ψ_2	0	0	1	0	0	−1	0	0	−1	0	0	1
Γ_7	Ψ_1	1	2	0	1	2	0	1	2	0	1	2	0
	Ψ_2	0	0	1	0	0	−1	0	0	1	0	0	−1
Γ_8	Ψ_1	1	0	0	1	0	0	−1	0	0	−1	0	0

triangular ab-plane lattice of dimers. Breaking of degeneracy should lead to an orthorhombic distortion of the hexagonal lattice. This was tested by an orthorhombic $Cmcm$ supercell to the low-temperature HRPD data, but no significant deviation of the a_o/b_o ratio was found, as shown in Fig. 3.

B. $Ba_3NdRu_2O_9$

A structural transition at 120 K and two probable spin-ordering transitions, at 24 and 17 K, were previously reported in this material.[11] Peak splittings consistent with the reported distortion from hexagonal $P6_3/mmc$ to monoclinic $C2/c$ symmetry at 120 K were observed in the low-temperature

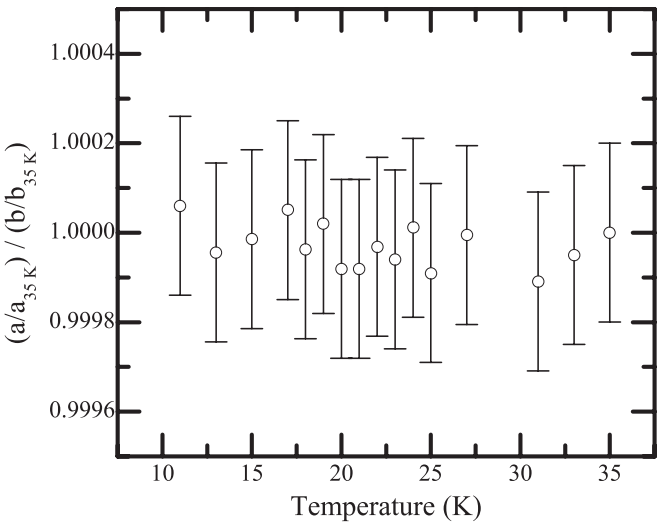

FIG. 3. Variation of the a/b lattice parameter ratio for $Ba_3LaRu_2O_9$ from Pawley (coordinate independent) fits in orthorhombic space group $Cmcm$ to high-resolution neutron powder diffraction data from HRPD at ISIS, normalized to the 35 K ratio. The normalized ratio does not deviate from unity on cooling through the 22 K magnetic ordering transition, showing that the lattice retains hexagonal symmetry within the resolution of the experiment.

x-ray diffraction patterns. The thermal evolution of lattice parameters extracted from Rietveld fits to the synchrotron powder diffraction data are plotted in Fig. 4(a). The angle β increases from 90° to around 90.9° on cooling through the transition, and the cell lengths vary monotonically down to the onset of magnetic order at 24 K. Lattice parameters in the range 1.6–30 K were extracted from the neutron powder diffraction data [Fig. 4(b)]. All four monoclinic lattice parameters have anomalies at $T_1 = 24$ K, and a further discontinuity at $T_2 = 18$ K is observed in the variation of the β angle.

To gain further insights into the structural transition in $Ba_3NdRu_2O_9$ and the structural anomalies accompanying the magnetic transitions, we have performed distortion mode analyses of the monoclinic structure with respect to the hexagonal parent $P6_3/mmc$ symmetry using the ISODISPLACE program[14] and the JEDIT interface[15] to the Rietveld refinement program TOPAS.[16] The results from fits to the synchrotron and neutron powder diffraction data are shown in Fig. 5. The distortion modes are labeled according to the site in $P6_3/mmc$ that they act on, and the symmetry of their order parameter direction. The Γ_6 modes are the primary order parameters for the structural phase transition as they have the largest amplitudes, and also because a Γ_6 distortion mode alone would imply the final $C2/c$ space group symmetry. The largest amplitude Γ_6 modes that emerge below the 120 K structural transition [Fig. 5(a)] involve the O2 oxygen atoms which are coordinated to the Nd^{3+} ions. The O2 sites also coordinate Ru, which may account for the large amplitude of the Γ_6(Ru) mode. Amplitudes from the neutron refinements in Fig. 5(b) show a large change in one of the Γ_4(O2) modes below the 25 K magnetic transition. The effects of this on the NdO_6 coordination octahedron are illustrated in Fig. 6. The Nd-O bond distances do not change significantly, but order-parameter-like changes in O-Nd-O bond angles occur below the 25 K transition. Refined structural parameters for $Ba_3NdRu_2O_9$ at 1.6 K are shown as Supplemental Material.[17]

Magnetic neutron diffraction peaks were observed below the previously reported $T_1 = 25$ K and $T_2 = 18$ K magnetic transitions.[11] Magnetic diffraction peaks [Fig. 7(a)] observed

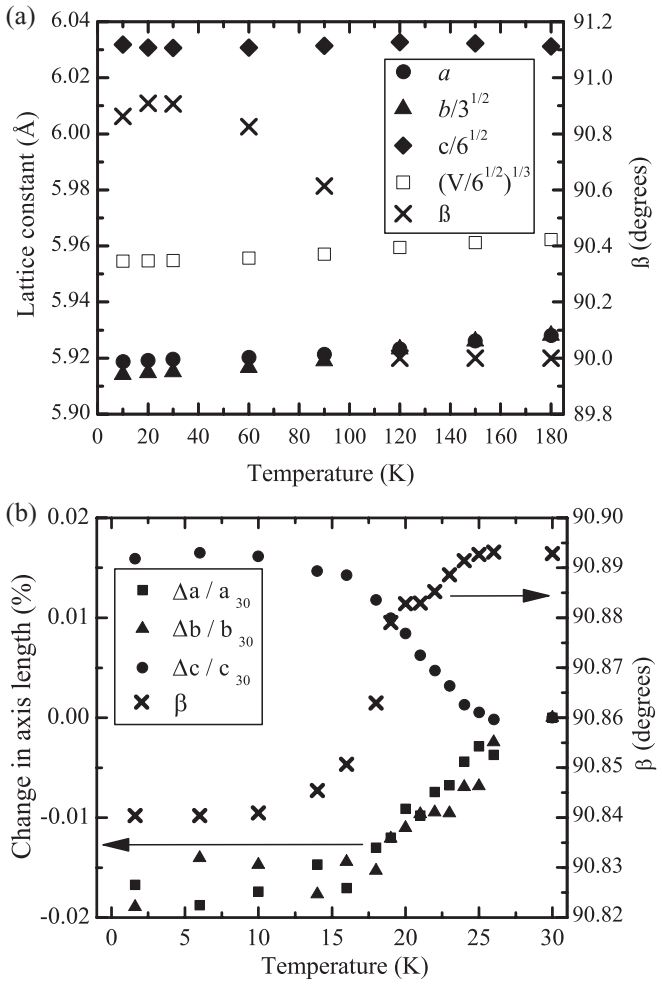

FIG. 4. Thermal evolution of lattice parameters for $Ba_3NdRu_2O_9$: (a) through the 120 K hexagonal to monoclinic phase transition, showing parameters from Rietveld fits to synchrotron powder x-ray diffraction data; (b) around the $T_1 = 24$ K and $T_2 = 18$ K magnetic transitions, using data from fits to neutron powder diffraction data, with changes in axis lengths relative to 30 K values of $a = 5.919\,97(3)$, $b = 10.250\,53(7)$, and $c = 14.772\,75(10)$ Å.

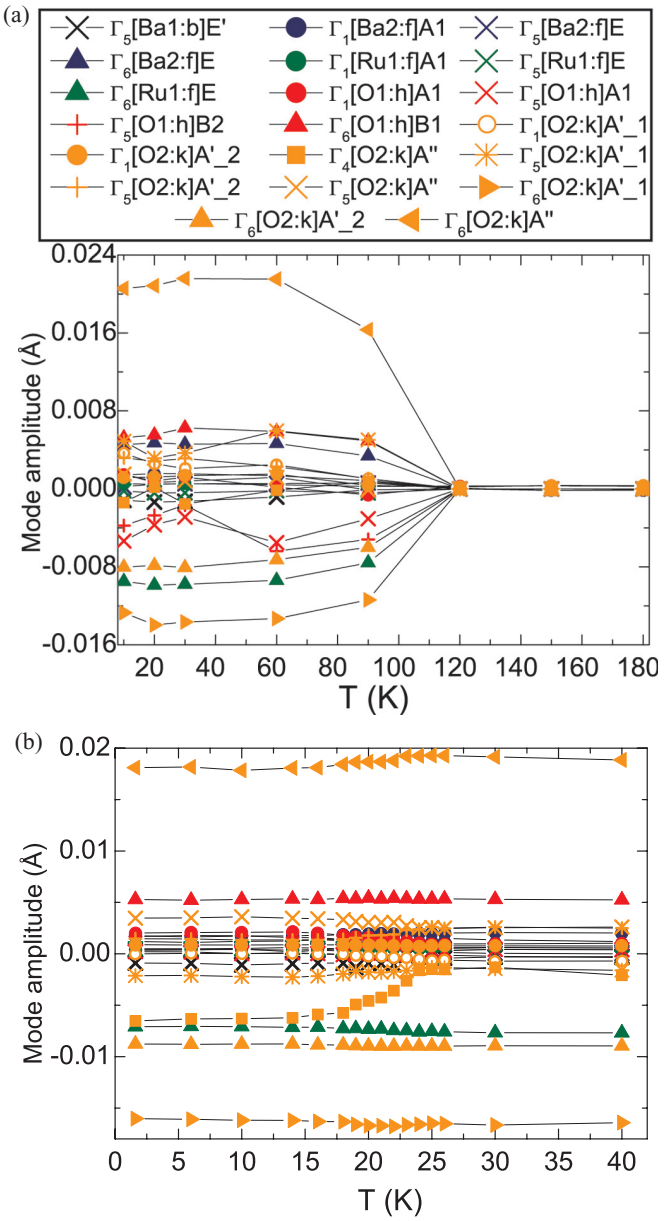

FIG. 5. (Color online) Thermal evolution of the distortion mode amplitudes for $Ba_3NdRu_2O_9$ from the refinements shown in Fig. 4. Distortion mode labels for both plots are shown above (a).

at 20 K indexed on a (0 0 0) propagation vector of the $C2/c$ cell. They were fitted by a ferromagnetic order of Nd^{3+} moments parallel to $\boldsymbol{c}$ [Fig. 7(b)], corresponding to the $\Psi_3(\Gamma_2)$ basis for (0 0 0) order in Table III. The refined magnitude of $1.56(7)\mu_B$ at 20 K is consistent with the previously published result obtained from neutron powder diffraction of $1.65(8)$ at 10 K.[11] No direct evidence for simultaneous ordering of Ru moments at T_1 is observed, although this is known to occur in materials such as the related double perovskite Ba_2NdRuO_6.[18] Fits to our data show that any ferromagnetically ordered Ru component has magnitude substantially lower than $0.4\mu_B$.

Below $T_2 = 18$ K, additional magnetic peaks characterized by two propagation vectors appear [Fig. 7(a)]. The (001) peak, which is systematically absent in the nuclear scattering, evidences a further, antiferromagnetic, (0 0 0) Nd spin component. This has refined magnitude $0.5(1)\mu_B$ at 1.6 K and can be modeled by a canting of the Nd moment along the $\boldsymbol{a}$ or $\boldsymbol{b}$ directions. Canting parallel to $\boldsymbol{b}$ is considered most likely as this is described by the $\Psi_2(\Gamma_2)$ basis vector belonging to the same representation as the ferromagnetic $\Psi_3(\Gamma_2)$ Nd spin component (Table III). Several further magnetic Bragg peaks ($\frac{1}{2}$ 1 2), ($\frac{1}{2}$ 1 1), and ($\frac{1}{2}$ 1 0) [Fig. 7(a)] that belong to the propagation vector ($\frac{1}{2}$ 0 0) were also observed. Symmetry analysis of the Ru sublattice in space group $C2/c$ under this propagation vector is summarized in Table III. The Ru site is split in this analysis, but the data available did not enable the two Ru spins to be fitted independently and only models with either a parallel or an antiparallel constraint on the moments within dimers were considered. A model of ferromagnetic Ru dimers, coupled antiferromagnetically to neighboring dimers [Fig. 7(c)], which transforms under Γ_1 of Table III, was found to give the best fit. This is equivalent to the ordered Ru:m_x components observed in $Ba_3LaRu_2O_9$ and $Ba_3YRu_2O_9$ above. However, there are still some discrepancies between observed and calculated

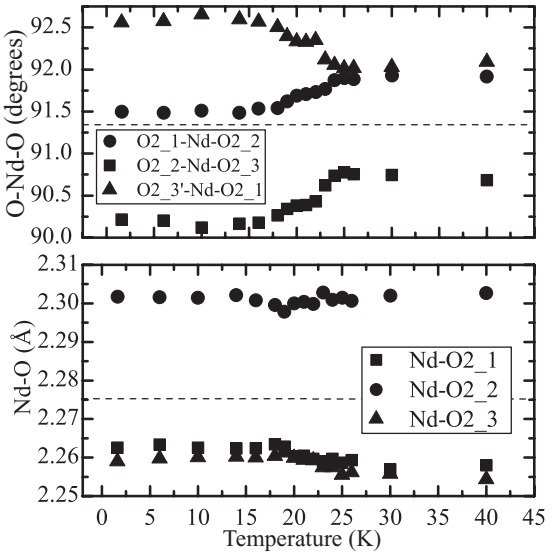

FIG. 6. Thermal evolution of the NdO_6 coordination environment in the monoclinic phase of $Ba_3NdRu_2O_9$ at low temperatures. Bond distances and angles are extracted from Rietveld fits to neutron powder diffraction data. The angles shown are equal above the 120 K structural transition, as are the distances.,

magnetic intensities, and a more extensive set of magnetic diffraction data would be needed to determine the full spin-ordered structure. The temperature evolution of the three $Ba_3NdRu_2O_9$ magnetic components is shown in Fig. 7(b). The ferromagnetic Nd:m_z(0 0 0) moment is an order parameter for the $T_1 = 25$ K transition, and the antiferromagnetic Nd:m_y (0 0 0) and Ru:$m_x(\frac{1}{2}\ 0\ 0)$ components have similar behavior below $T_2 = 18$ K.

Magnetization-field loops for $Ba_3NdRu_2O_9$ are shown in Fig. 7(d). The saturated moment of $\sim 1.2\mu_B$/formula unit at 2–20 K is comparable to the magnitude of the ordered ferromagnetic Nd:m_z(0 0 0) component. A simple hysteresis loop with little coercivity is observed at 15 and 20 K, but a substantial coercive field of 1.1 T is observed at 2 K. In addition, $\frac{1}{3}$ (of maximum) -magnetization steps are observed in the 2 K loop. These evidence coherent reversal of ferromagnetic Nd chains or planes, as discussed later.

IV. DISCUSSION

Magnetic neutron diffraction shows that ferromagnetic Ru spin dimers are present in all of the $Ba_3B'Ru_2O_9$ (B' = La, Nd, Y) ground states. This is in contrast to predictions for these materials,[3] and to observations of antiferromagnetic dimers in $B' = Co^{2+}$ and Ni^{2+} materials[8] and evidence for antiferromagnetic or spin-singlet $(Ru^{5+})_2$ and $(Ru^{6+})_2$ dimers in charge-ordered $Ba_3NaRu_2O_9$.[6] The key difference is that the Ru ions in the latter materials have integral charge states, whereas in the rare earth series an average $Ru^{4.5+}$ state is apparent with no evidence for charge ordering. Ferromagnetism is favored by delocalization of the single minority (down-)spin t_{2g} electron in each dimer, so the idealized orbital populations are $t_{2g}(\uparrow)^3\, t_{2g}(\downarrow)^{0.5}$. This is a molecular example of the double (Zener) exchange interaction observed in mixed valent manganese oxide perovskites such as $La_{0.7}Sr_{0.3}MnO_3$. The short Ru-Ru separation in the dimers ($D_{\text{Ru-Ru}} \sim 2.5$ Å) facilitates this direct interaction between the t_{2g} orbitals.

The same antiferromagnetic order of ferromagnetic Ru dimers is observed in $Ba_3B'^{3+}Ru_2O_9$ for B' = Y, Nd, and La, but the respective ordering temperatures of 4.5, 18, and 22 K vary markedly. This is attributed to a lattice effect controlled by the B'^{3+} cation size—such sensitivity is typical in perovskite-related oxides.[19,20] Figure 8 shows that the magnetic ordering temperature (reported Néel temperatures for B' = rare earth and Y;[3] the value for Bi^{3+} is assigned from the magnetic heat capacity;[7] spin freezing transition for $B' = In^{3+}$)[1] increases smoothly with the ionic radius of B'. This variation implies that the same antiferromagnetic arrangement of ferromagnetic dimers is present throughout the series. The observed $T_2 = 18$ K of $Ba_3NdRu_2O_9$ follows the trend for the other $Ba_3B'^{3+}Ru_2O_9$ materials in Fig. 8, showing that the lattice distortion and ordering of Nd moments at higher temperatures appear not to perturb the Ru spin order.

Although the observed long-range spin order breaks the triangular degeneracy of the lattice, no evidence for an orthorhombic distortion of the hexagonal lattice is evident in $Ba_3LaRu_2O_9$ (Fig. 3), which has the highest T_N of the B' = rare earth series. Hence, the increase in T_N with B' size does not result from relief of magnetic frustration, and is probably related to geometric enhancement of superexchange interactions between dimers.

TABLE III. Irreducible representations and basis vectors of the space group $C2/c$ for Ru at $(x,y,z) = (0.994, 0.332, 0.836)$[11] under propagation vector $(\frac{1}{2}\ 0\ 0)$, and for Nd at (0,0,0) under vector (0 0 0), in $Ba_3NdRu_2O_9$. Ru is split into independent sites shown as Ru_1 and Ru_2. $\Psi_3(\Gamma_2)$ and $\Psi_2(\Gamma_2)$ respectively describe the ferromagnetic (at T_1) and antiferromagnetic (at T_2) orders of Nd moments under propagation vector (0 0 0), and $\Psi_1(\Gamma_1)$ was used for the $(\frac{1}{2}\ 0\ 0)$ magnetic order of Ru moments at T_2.

Irreducible representations	Basis vectors	$Ru_1(x, y, z)/Ru_2(-x, y, -z+\frac{1}{2})/Nd(x, y, z)$			$Ru_2(x, -y, z+\frac{1}{2})/Ru_1(-x, -y, -z)/Nd(-x, y, -z+\frac{1}{2})$		
		m_x	m_y	m_z	m_x	m_y	m_z
Γ_1	Ψ_1	1	0	0	−1	0	0
	Ψ_2	0	1	0	0	1	0
	Ψ_3	0	0	1	0	0	−1
Γ_2	Ψ_1	1	0	0	1	0	0
	Ψ_2	0	1	0	0	−1	0
	Ψ_3	0	0	1	0	0	1

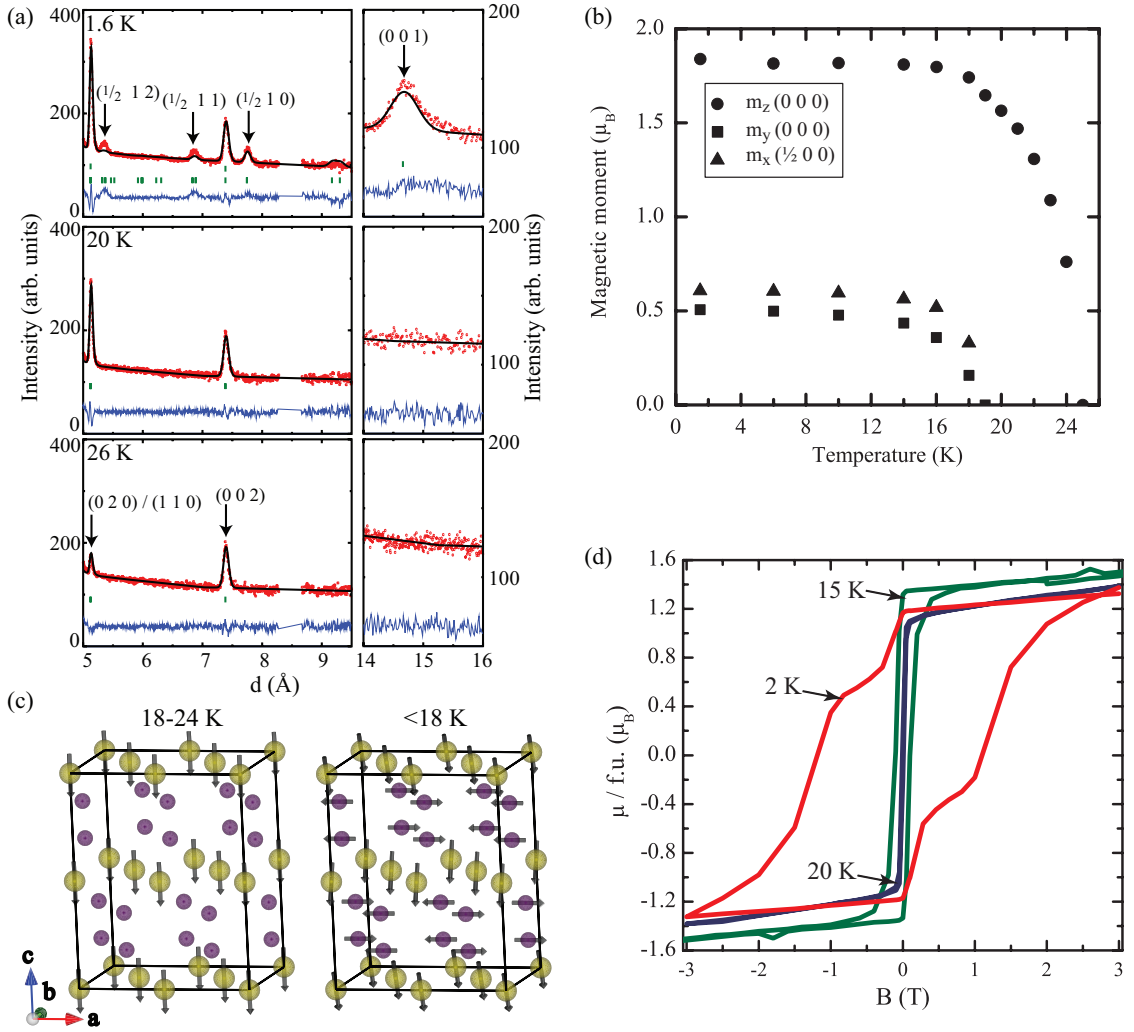

FIG. 7. (Color online) Magnetic ordering results for $Ba_3NdRu_2O_9$. (a) Fits to regions of the neutron diffraction data from $2\theta = 58^\circ$ (left) and 27° (right) detector banks of WISH at ISIS. Ferromagnetic order of Nd moments at $T_1 = 24$ K is evidenced by the enhancement of (110) intensity on cooling from 26 to 20 K. $(\frac{1}{2}\ 1\ l)$ peaks from Ru spin order and (001) from Nd spin canting emerge on cooling through $T_2 = 18$ K. (b) Thermal evolution of Nd $\Psi_3(\Gamma_2)$ $m_z(0\ 0\ 0)$ and $\Psi_2(\Gamma_2)$ $m_y(0\ 0\ 0)$, and Ru $\Psi_1(\Gamma_1)$ $m_x(0\ 0\ \frac{1}{2})$ spin components. (c) Magnetic structures between T_1 and T_2 (left) and below T_2, showing Nd/Ru as large/small atoms. (d) Magnetic hysteresis loops at 2, 15, and 20 K, showing $\frac{1}{3}$-magnetization steps at 2 K.

$Ba_3NdRu_2O_9$ is remarkable in displaying a lattice distortion at a relatively high temperature (120 K) that is not observed in any of the other $Ba_3B'Ru_2O_9$ (B'^{3+} = rare earth) materials.[3] This is clearly not a size-driven effect, as the analogs with larger B' = La and smaller B' = Y both remain hexagonal down to at least 2 K. Crystal-field effects on $4f^n$ rare earth ion lattices are usually weak, but are the only plausible explanation for the anomalous lattice behavior of $Ba_3NdRu_2O_9$. The $^4I_{9/2}$ ground state of $4f^3$ Nd^{3+} splits into five Kramers doublets, and the lowest two in energy are degenerate in an octahedral crystal field, and so this environment is sensitive to Jahn-Teller distortion. This is corroborated by our structural data in Figs. 4 and 5, which show that the largest distortion amplitudes at the 120 K transition are predominantly Γ_6 modes associated with local deformations of the NdO_6 octahedra. These break the equivalence of Nd-O distances and O-Nd-O angles (Fig. 6).

Magnetic order of the Nd^{3+} spins induces further lattice distortion through spin-orbit coupling, as evidenced by the cell parameter anomalies at the magnetic T_1 and T_2 transitions shown in Fig. 4(b). The distortion mode analysis in Fig. 5(b) demonstrates that a Γ_4 distortion of the NdO_6 octahedra is the main internal order parameter for the additional deformation below the $T_1 = 24$ K onset of magnet order. This twisting deformation creates further disparity between O-Nd-O angles but does not affect the Nd-O distances.

The presence of lattice distortions and two magnetically active cations makes analysis of the spin order in $Ba_3NdRu_2O_9$ more complex than that in the La and Y analogs, but the main features are clear from the present powder neutron study. The $T_1 = 24$ K transition corresponds to a ferromagnetic order of only Nd^{3+} spins, parallel to the c axis. Two antiferromagnetic modes emerge at the $T_2 = 18$ K transition. The

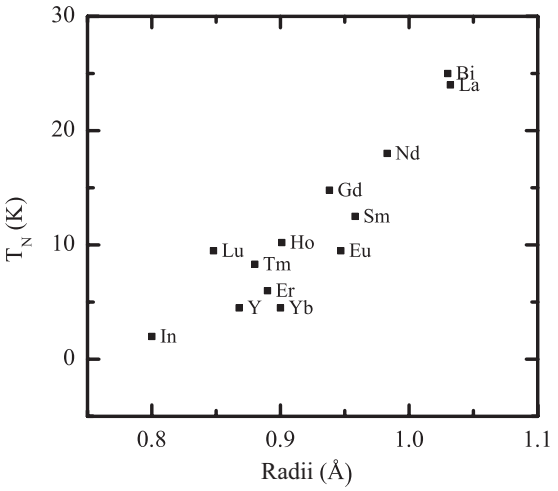

FIG. 8. Plot of the reported Ru spin-ordering temperatures of 6H-perovskites $Ba_3B'Ru_2O_9$ against ionic radius of the trivalent B' ions.

antiferromagnetic order of Ru dimers is like that observed in $Ba_3LaRu_2O_9$ and $Ba_3YRu_2O_9$, and this induces a further antiferromagnetic component to the Nd^{3+} spin order, corresponding to an overall canting of the moments. The concomitant ordering of two modes that belong to different propagation vectors implies coupling between the two propagation vectors, which would necessitate a doubling of the Γ point such that it contains both representations. This may account for why a complete description of the magnetic structure is not achieved within the present representational analysis. Simulated annealing of the magnetic structure in a larger supercell (containing eight Nd and 16 Ru sites) was attempted but did not lead to any physically reasonable solutions. Complex magnetic orders with narrow temperature windows between successive transitions are common in metallic rare earth compounds,[21] but are unusual in insulating rare earth–transition metal oxides.

The lattice distortions of $Ba_3NdRu_2O_9$ evidently create a substantial anisotropy, as a large magnetic coercivity is observed at 2 K [Fig. 7(d)] and the reversal of magnetization proceeds via $\frac{1}{3}$-magnetization steps; ↑↑↑→↑↓↑→↓↓↓→↓↑↓→↑↑↑ as magnetic field is cycled up → down → up. Two models for the ↑↓↑ $\frac{1}{3}$-magnetization phase are plausible—an order of 2↑:1↓-spin chains parallel to the c axis, as observed in some frustrated triangular lattices such as CoV_2O_6,[22–24] or an ↑↓↑ order of successive Nd planes perpendicular to $\boldsymbol{c}$. High-field neutron diffraction will be needed to distinguish between these possibilities.

V. CONCLUSIONS

Ferromagnetic Ru spin dimers are present in $Ba_3B'Ru_2O_9$ (B' = La, Nd, Y), in contrast to antiferromagnetic dimers reported in other $Ba_3B'Ru_2O_9$ types, evidencing an intradimer double exchange coupling. Antiferromagnetic order of the dimers breaks the degeneracy of the frustrated triangular lattice, but no accompanying lattice distortion is observed. $Ba_3NdRu_2O_9$ is unique among the B' = rare earth series as it undergoes a structural distortion driven by Nd^{3+} crystal-field effects, and a separate ferromagnetic transition at lower temperatures. A substantial magnetic anisotropy leads to large coercivity and $\frac{1}{3}$-magnetization steps in the magnetic hysteresis of $Ba_3NdRu_2O_9$ at low temperatures.

ACKNOWLEDGMENTS

We thank Dr A. Daoud-Aladine and Dr P. Manuel for beamline support at ISIS. We acknowledge EPSRC, STFC, the Leverhulme Trust, and the Royal Society for support and the provision of ISIS and ESRF beam time.

*Current address: Johnson Matthey Technology Centre, Savannah, GA, USA.
†j.p.attfield@ed.ac.uk

[1] L. Shlyk, S. Kryukov, V. Durairaj, S. Parkin, G. Cao, and L. E. De Long, J. Magn. Magn. Mater. **319**, 64 (2007).
[2] H. D. Zhou, E. S. Choi, G. Li, L. Balicas, C. R. Wiebe, Y. Qiu, J. R. D. Copley, and J. S. Gardner, Phys. Rev. Lett. **106**, 147204 (2011).
[3] Y. Hinatsu and Y. Doi, Bull. Chem. Soc. Jpn. **76**, 1093 (2003).
[4] H. W. Zandbergen and D. J. W. Ijdo, Acta Crystallogr., Sect. C **40**, 919 (1984).
[5] J. T. Rijssenbeek, Q. Huang, R. W. Erwin, H. W. Zandbergen, and R. J. Cava, J. Solid State Chem. **146**, 65 (1999).
[6] S. A. J. Kimber, M. S. Senn, S. Fratini, H. Wu, A. H. Hill, P. Manuel, J. P. Attfield, D. N. Argyriou, and P. F. Henry, Phys. Rev. Lett. **108**, 217205 (2012).
[7] W. Miiller, M. Avdeev, Q. Zhou, A. J. Studer, B. J. Kennedy, G. J. Kearley, and C. D. Ling, Phys. Rev. B **84**, 220406(R) (2011).
[8] P. Lightfoot and P. D. Battle, J. Solid State Chem. **89**, 174 (1990).
[9] H. D. Zhou, A. Kiswandhi, Y. Barlas, J. S. Brooks, T. Siegrist, G. Li, L. Balicas, J. G. Cheng, and F. Rivadulla, Phys. Rev. B **85**, 041201 (2012).
[10] Y. Doi, K. Matsuhira, and Y. Hinatsu, J. Solid State Chem. **165**, 317 (2002).
[11] Y. Doi, Y. Hinatsu, Y. Shimojo, and Y. Ishii, J. Solid State Chem. **161**, 113 (2001).
[12] L. C. Chapon, P. Manuel, P. G. Radaelli, C. Benson, L. Perrott, S. Ansell, N. Rhodes, D. Raspino, D. Duxbury, E. Spill, and J. Norris, Neutron News **22**, 22 (2011).
[13] J. Rodriguez-Carvajal, Physica B **55**, 192 (1993).
[14] B. J. Campbell, H. T. Stokes, D. E. Tanner, and D. M. Hatch, J. Appl. Crystallogr. **39**, 607 (2006).
[15] J. S. O. Evans, Mater. Sci. Forum **651**, 1 (2010).
[16] A. A. Coelho, J. Appl. Cryst. **36**, 86 (2003).
[17] See Supplemental Material at http://link.aps.org/supplemental/10.1103/PhysRevB.87.134402 for refined structural parameters of $Ba_3NdRu_2O_9$ from refinement against 1.6 K powder neutron diffraction data.

[18] Y. Izumiyama, Y. Doi, M. Wakeshima, Y. Hinatsu, K. Oikawa, Y. Shimojo, and Y. Morii, J. Mater. Chem. **10**, 2364 (2000).
[19] J. P. Attfield, Int. J. Inorg. Mater. **3**, 1147 (2001).
[20] J. P. Attfield, Cryst. Eng. **5**, 427 (2002).
[21] J. van Duijn, J. P. Attfield, and K. Suzuki, Phys. Rev. B **62**, 6410 (2000).
[22] S. A. J. Kimber, H. Mutka, T. Chatterji, T. Hofmann, P. F. Henry, H. N. Bordallo, D. N. Argyriou, and J. P. Attfield, Phys. Rev. B **84**, 104425 (2011).
[23] M. Markkula, A. M. Arevalo-Lopez, and J. P. Attfield, J. Solid State Chem. **192**, 390 (2012).
[24] M. Markkula, A. M. Arevalo-Lopez, and J. P. Attfield, Phys. Rev. B **86**, 134401 (2012).